Journal of Colloid and Interface Science 322 (2008) 365–374

Contents lists available at ScienceDirect

Journal of Colloid and Interface Science

www.elsevier.com/locate/jcis

Adsorption of copolymers aggregates: From kinetics to adsorbed layer structure

Bogdan Zdyrko [a], Pazit Bar-Yosef Ofir [a], Alina M. Alb [b], Wayne F. Reed [b], Maria M. Santore [a,*]

[a] Department of Polymer Science and Engineering, University of Massachusetts, 120 Governors Drive, Amherst, MA 01003, USA
[b] Department of Physics, Tulane University, New Orleans, LA 70118, USA

ARTICLE INFO

Article history:
Received 7 January 2008
Accepted 26 March 2008
Available online 7 April 2008

Keywords:
Polymer brush adsorption
Aggregate adsorption
Micelle adsorption
Associated adsorbed layer
Mushroom layer
Adsorbed copolymers
Copolymer layers
Adsorption kinetics

ABSTRACT

We examined the adsorption, on hydrophobic and hydrophilic surfaces, of 4 rake-type poly(dimethyl siloxane) (PDMS) copolymers varying the amount of poly(ethylene glycol) (PEG) graft arms from 41 to 72%. The copolymers formed large aggregates in solution, complicating their adsorption kinetics and layer structures. We found the adsorption process always to be dominated by the adsorption of large aggregates, with strongly bound layers resistant to rinsing in adsorbing buffer. Adsorbed amounts were nearly independent of the substrate. However, subtleties in the adsorption kinetics suggested different layer structures for the different systems. On hydrophilic silica, aggregates adsorbed at the transport limited rate until surface saturation, and associated interfacial structures were likely retained. On the hydrophobic surface, a subset of the copolymers exhibited retarded late stage adsorption kinetics suggestive of brush formation. This work demonstrates how subtle differences in adsorption kinetics provide insight into potential interfacial layer structures.

1. Introduction

Sophisticated biomedical applications such as implants and chip-based diagnostics demand bio-inert surfaces, and the past several decades have seen major advances in surface-initiated polymerizations to grow brushes *from* surfaces [1]. Surface-grown brushes possess chain densities that potentially meet needs for protein resistance and more [2]; however, some applications requiring bio-inert surfaces may not be able to exploit brush-growth-from-surface methods, for reasons of scale, chemistry, or economy. Here, the classical approach of polymer adsorption represents the most promising option to protect surfaces from proteins and avoid cell adhesion. Indeed, adsorbing polymers have retained their technological niche to maintain dispersion stability and modify macroscopic surfaces. Now, there is renewed interest in polymer adsorption, with greater focus on protein resistance and bioadhesion. The construct of adsorbed polymer brushes and the ability to place them on a variety of surfaces is more important than ever.

Polyethylene glycol (PEG) or polyethylene oxide (PEO) remains a popular choice for surface biocompatibilization. Of the approaches for surface "pegylation" [3–14], those that produce robust dense polymer brushes most effectively resist proteins [3,5,6,8,11]. (We distinguish between over-packed protein-adhesive PEG-terminated SAMs [15–17] and the practical challenge of placing enough PEG chains on the surface to render it bioinert.) Because PEG chains are readily displaced by adsorbing proteins, the formation of PEG brushes requires anchoring PEG chains to a surface using sticky end groups. This can be achieved, for instance by a copolymer block that is attracted to the surface. Copolymer adsorption to produce PEG brushes proceeds rapidly at first; but ultimately, adsorbed PEG chains present an osmotic barrier [18] against the approach of additional chains, protracting the timescale of brush development [19–22]. This effect can be reduced by employing solution concentrations above c^* or lowering solvent quality to facilitate penetration of new chains into the growing brush [23]; however, most brushes formed by adsorption do not quantitatively meet the classical description [24], as a result of low surface coverage or adsorption of the intended tether [2,25,26].

PEG-hydrophobe copolymers and surfactants, though practical and economical (and commercially available!) choices for PEG brushes, present a special challenge: They tend to micellize in aqueous solution and may associate in an adsorbed layer, producing surface morphologies other than brushes. Establishing a robust PEG brush requires a large hydrophobic anchor (providing adsorption energy to balance the corona stretching energy [24,25]), which in turn increases the probability of micelle formation, and lowers the CMC. Further, the proportions of hydrophobic versus PEG blocks may favor curved interfaces between the condensed hydrophobic core and the hydrated PEG corona, so that micelles are retained interfacially, in some form. All this leads to both equilibrium and dynamic considerations (which may be at odds) for choosing chains of a particular architecture or hydrophobic content for (attempted) brush adsorption.

* Corresponding author.
E-mail address: santore@mail.pse.umass.edu (M.M. Santore).

0021-9797/$ – see front matter
doi:10.1016/j.jcis.2008.03.047

The questions remain, then, to what extent can useful brushes be formed by adsorption of commercial hydrophobe-PEG copolymers, and how do solution-phase structures and interfacial dynamics affect the ultimate interphase? With model hydrophilic and hydrophobic substrates, the current study examines the adsorbed layer formation process for a series of siloxane-based rake-copolymers for which the amount of polyethylene glycol (PEG) side chains is varied. Siloxane-based surfactants and copolymers have been studied mostly in the context of wetting agents and superspreaders [27–30], with limited reports focusing on their ability to form adsorbed layers [31,32]. Of the few adsorption studies with rake PEG–siloxane copolymers, one reports similarities between solution and adsorbed layer structures [31], while another finds long-lived surface micelles on hydrophilic surfaces [33,34]. Though the copolymers studied here are not identical to those of the other studies, their highly hydrophobic backbones (with molecular weight order 1000, greater than the alkane molecular weights of most simple surfactants) drive micelle and aggregate formation at relatively low concentrations, complicating the both the layer formation dynamics and structure. The current work therefore draws attention to subtle differences in adsorption kinetics that must arise from structural differences in the growing layers. As not all systems are readily amenable to sophisticated probes of layer structure such as AFM and neutron reflectivity, the kinetic results, combined with some knowledge of the behavior of model systems from the literature, provide insight into possible layer structures.

We report here that, for all the copolymers studied, the solution phase structures (micelles and aggregates) dominate the adsorption process and affect layer structure in different ways for hydrophobic and hydrophilic surfaces. Estimates, based on mass-transport limited adsorption, of aggregate and micelle sizes corroborated light scattering data, confirming the identity of the dominant adsorbing species. Substrate hydrophobicity had a very small effect on the ultimate adsorbed amounts of the 4 surfactants, giving the impression of identical layers on the two kinds of surfaces; however, subtle differences in the late-stage kinetics suggest substantial differences in layer structure. A slow approach to saturation, seen only for the most hydrophilic copolymers adsorbing on the hydrophobic surface, was suggestive of brush formation, while surface micelles and aggregates were more likely on hydrophilic surfaces or with more hydrophobic copolymers.

While a number of fundamental experimental studies have focused on structural, and to a lesser extent kinetic features of brush formation by adsorption [35–37], this work distinguishes itself because it focuses on systems dominated by aggregates. A subset of the literature considers single molecule versus micelle adsorption [38–41], and notes differences in the adsorbed amounts that relate to layer structure; however, the current study differs in that the adsorbing siloxane backbone is highly mobile relative to the polystyrene adsorbing block of these prior studies. As a result the current aggregates in solution equilibrate rapidly and their adsorbed layers may follow suit. The systems studied here also differ dramatically from the much-studied pluronic series [42] whose poly(propylene oxide) mid-block lacks the hydrophobicity of siloxane, and hence immense aggregated structures are not seen for the former.

The adsorbed layers in this work are ultimately classified as aggregated, brush, or aggregate-on-mushroom structures, based on combined kinetic and coverage data. We report separately [43], on the protein-resistance of these layers, with those systems of brush structure providing the greatest resistance to protein adsorption.

Table 1
PEG-PDMS copolymers (*from Dow Corning product literature*)

Copolymer name	Architecture	Total M_w	M_w PDMS	M_w PEG	PEG (wt%)
DC-193	Rake	3100	868	2232	72%
DC-5103	Rake	2500	875	1625	65%
DC-5097	Rake	2300	1081	1219	53%
DC2-8692	Triblock	1900	1121	779	42%

2. Experimental details

2.1. Materials

The four commercial "surfactants" from Dow Corning, listed in Table 1, are copolymers of poly(dimethylsiloxane) (PDMS) and poly(ethylene glycol) (PEG). Three are graft architecture and one is a triblock (PEG–PDMS–PEG), varying their PEG content at nearly constant PDMS backbone molecular weight. Despite their commercial polydispersity, orders of magnitude differences in the size of the solution phase structures (micelles and aggregates) result from less than a factor of 2 difference in PEG content. We also note that these commercial copolymer may also contain "contaminant" species, for instance free PEG (EO-12) oligomers. We have confirmed, however, that 500 molecular PEG does not adsorb significantly to either hydrophobic monolayers or hydrophilic silica, and therefore does not interfere with our results.

Of note for the two most hydrophilic polymers, DC-193 and DC-5103, the nominal backbone molecular weight is nearly identical, but the PEG molecular weight is greater for the DC-193 by about 700–800 units. DC-193 is denoted, by Dow Corning, to be a polyoxamer 12 (i.e. the PEG arms are nominally 12 units, or 530 molecular weight). This suggests that the DC193 contains, on average 1–2 more side arms (4–5 total) compared with the DC-5103 (about 3 arms total). The series also contains a triblock copolymer as its most hydrophobic member. In the limit of the more hydrophobic compounds in the series, there can only be 2–3 side arms on the graft copolymers, thus the distinction between graft and triblock architectures becomes small. One might therefore expect a coherent trend among all 4 compounds in Table 1.

Experiments employed copolymer solutions in pH 7.4 phosphate buffer, 0.008 M Na_2HPO_4 and 0.002 M KH_2PO_4, from Fisher.

Silica was chosen as a model hydrophilic surface, generated by soaking microscope slides (Fisher Finest) in concentrated sulfuric acid overnight. This procedure has been shown to remove sodium and other metal ions from the surface, leaving a surface region of pure silica, on the order of 10 nm thick [44].

C16 monolayers were chosen as the model hydrophobic surface. These were formed on microscope slides that had been immersed in freshly prepared piranha solution (30 of 30% hydrogen peroxide and 70% of concentrated sulfuric acid 98%, both from Fisher Scientific) for 30 min. After the piranha treatment, slides were rinsed with copious amounts of DI water and dried under nitrogen. Slides were then immediately immersed in 0.4% (v/v) trichlorohexadecyl silane (Gelest) in dry toluene (Fisher, water content less than 0.03%). After 4 h of reaction at room temperature, slides were rinsed three times with toluene, and sonicated for 5 min in toluene. The slides were then heated for 10 min at 120 °C. The surface quality was monitored via water contact angle. Samples whose advancing contact angles were between 105°–110° were used for adsorption studies.

2.2. Methods

Surface tension measurements were made via pendant drop shape analysis on a contact angle goniometer (Kruss Model DSA10), employing copolymer solutions over a broad range of concentrations.

Copolymer solutions were also characterized via static light scattering, using the Automatic Continuous Mixing (ACM) approach [45,46]. A Shimadzu gradient pump was used to create a continuous ramp of copolymer concentration, and the scattering intensity of this flowing solution was measured simultaneously at seven angles using a Brookhaven Instruments Corporation BI-MwA. A Shimadzu VP10 refractive index detector, in series with the BI-MwA, monitored the polymer concentration in the ramp. Data analysis methods have been detailed previously, and are based on obtaining a weight-average molar mass, M_w, z-averaged mean square radius of gyration $\langle S^2\rangle_z$, and second virial coefficient, A_2. For convenience, "radius of gyration" will refer to the root mean z-averaged square radius of gyration, $\langle S^2\rangle_z^{1/2}$. A custom-built single capillary viscosity detector was also placed in series with the other detectors.

Adsorption was measured using near-Brewster reflectometry in an internal back-reflection configuration [44]. Here a parallel-polarized HeNe (633 nm) laser impinges, through the substrate, on the solid–liquid interface. The intensity of the back reflected beam, which is very nearly zero near the Brewster angle, increases with the adsorbed amount, which is calculated from a 2-layer optical model in which a silica layer on the outermost surface of the glass, and the adsorbed copolymer itself comprise the two layers. The adsorption studies themselves were conducted in slit-shear cells through which a gentle shearing flow was maintained (here 5 s^{-1}). A black Teflon block comprised the base of the cell and a microscope side (acid etched or C16 surface), was clamped against an o-ring to make one wall of the flow chamber.

3. Results

3.1. Characterization of copolymers

Fig. 1 reports the surface tensions of aqueous copolymer solutions over several decades, used to guide the choice of concentrations for this study. As expected, all 4 compounds are surface active, but do not exhibit a clear CMC. This is consistent with the possibility of structures more complicated than simple micelles.

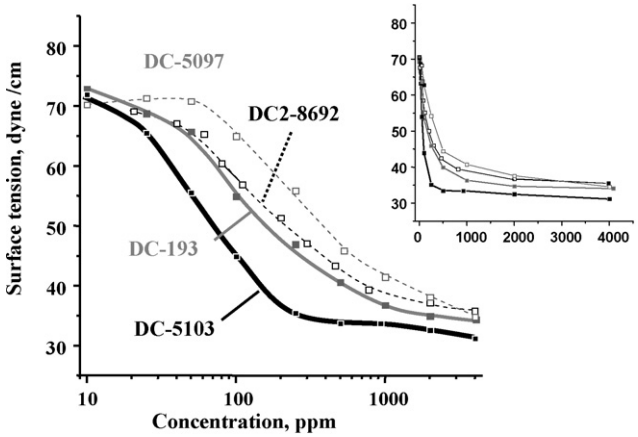

Fig. 1. Surface tensions of surfactant solutions Main graph is semi-log; inset is linear.

Light scattering provides further insight into the solution-phase structures, in Table 2. All 4 copolymers form highly-scattering aggregates, and this is especially pronounced for DC-5107 and DC2-8692 which scatter well over an order of magnitude more at low angles than DC-193 or DC-5103. Indeed, solutions of all 4 copolymers exhibit strong scattering even in the most dilute regime, below 20 ppm, indicating the presence of aggregates at all measurable concentrations. This finding runs against classical thinking for the shapes of the surface tension curves of Fig. 1; however, surface tension measures the activity of species at the air–water interface, not solution structure. The fact that Fig. 1 shows the main decrease in surface tension to occur near 100 ppm rather than far below may suggest that there is very little copolymer (ever!) in the form of single molecules. Aggregates at the air–water interface would have a smaller effect on the energy of that interface than individual molecules.

Further evidence for dominance of the solution by large colloidal aggregates follows from the lack of measurable viscosity signal from any of the solutions. This is characteristic of massive, dense particles, and consistent with the near-zero A_2 of DC-193, DC-5103, and DC-5097. (Though any polymer in a theta solvent will yield a zero A_2, it is also typical of aggregates to have very small A_2 values, which is a measure of excluded volume per molar mass squared.) The concentration range over which A_2 was determined is also included in Table 2: Whereas DC-193 and DC-5103 yielded behavior within the Rayleigh–Debye approximation [47], the DC-5097 and DC2-8692 are too large for the approximations to hold, so that aggregate size and A_2 are approximated semi-quantitatively.

DC-193 forms objects 40 nm in radius, much larger and more massive ($M_w \sim 10^5$ g/mol) than expected for micelles, given the small size of the individual copolymer chains. Polydispersity is suggested by the fact that the observed radius is even larger than expected for the measured aggregate molecular weight. $\langle S^2\rangle_z^{1/2}$ therefore represents the large size portion of the population while M_w is weighted toward smaller masses. The DC-5103 is similar to the DC-193, but more massive (5×10^5 g/mol) and yet somewhat smaller, indicating a more dense particle, still polydisperse. As the amount of hydrophilic side arms is further reduced, DC-5097 and DC2-8692, the aggregates grow dramatically.

There was evidence in each case that as the copolymer concentration increased, A_2 became more positive, and that upwards curvature of the reciprocal scattering versus concentration suggested the effects of a third virial coefficient, A_3. Although we do not wish to over-interpret the data, this suggests that the morphology of the structures may change with increasing concentration, yielding entities that have stronger repulsive interactions than those at low concentration.

While one might worry about the significance of such solution phase structures, i.e. their history dependence or whether they represent equilibrium, we make the following comment. The solutions employed here gave the same light scattering results and adsorption behaviors after months of storage, with no history dependence. The aggregate structure was not seen to evolve with time. Further, these light scattering results, which are done via dilution of a stock solution with pH 7 phosphate buffer to produce ramp-wise concentration variations just upstream of a scattering

Table 2
Light scattering from copolymer solutions

Copolymer	PEG (wt%)	M_w (aggregate)	A_2 (mol-cm^3/g^2)[a]	C_{max} (g/cm^3)	$\langle S^2\rangle z^{1/2}$ (nm)
DC-193	72%	120,000	~0	10^{-3}	40
DC-5103	65%	580,000	~0	4×10^{-4}	20
DC-5097	53%	$>10^8$	$\sim 5 \times 10^{-5}$	2×10^{-4}	100 ± 25
DC2-8692	42%	$>10^8$	$\sim 10^{-3}$	6×10^{-5}	>200

[a] A_2 determined from $C = 0$ up to C_{max}.

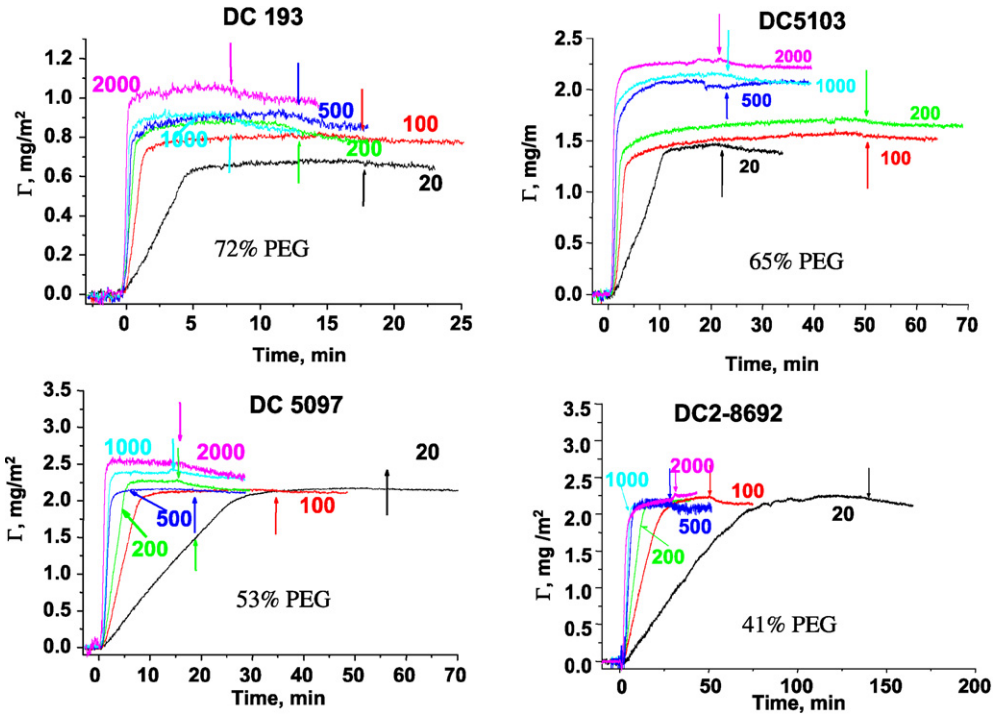

Fig. 2. Raw adsorption traces on silica surface. Arrows denote buffer reinjection. Data sets (DC-193 200 ppm, 1000 ppm; DC2-8692 1000 ppm) have been omitted for black and white viewing. (For printed version only.)

detector, gave identical results regardless of the initial concentration of the concentrated stock solution. This indicates a rapid structural equilibration suggesting that the solution structures, if not completely equilibrated, represent a highly stable metastable state.

3.2. Adsorption on silica

Fig. 2 illustrates the adsorption traces of all 4 copolymers on silica. For each copolymer, adsorption was studied at 6 concentrations from 20 ppm to 2000 ppm, based on the important range identified in Fig. 1. Multiple runs were conducted with each compound, and Fig. 2 shows representative results. For each run, flowing buffer (at a modest wall shear rate of 5 s^{-1}) was monitored for 10 min or more to establish a stable baseline. Then, following a valve turnover, buffered copolymer solution was pumped through the cell. The signal increased as adsorption commenced. Once a plateau was established, suggesting surface saturation, buffer was again pumped through the cell to determine if any copolymer desorbed on short timescales.

Fig. 2 exhibits several important features. First, in all cases, the signal rise is linear, and the initial adsorption rates increase with increasing bulk solution concentration, (consistent with transport-limited kinetics). For nearly all the runs, saturation of the surface occurs rather abruptly with a sharp shoulder, indicating that, even when the surface is crowded, adsorption still occurs quickly (at the transport-limited rate, it turns out) until complete saturation. (A possibility is that, with the highly flexible PEG and PDMS constituents, rapid chain motions ensure that the relaxation timescale of the layer is at least as fast as the timescale for mass accumulation at the interface.) Another important observation, there is little or no removal of copolymer when the adsorbed layers are exposed to flowing buffer. (Buffer injection is indicated by an arrow for each run.) Thus, all copolymers are fairly strongly adsorbed to silica.

Fig. 2 also shows that the timescales for adsorption and establishing the ultimate coverages are strongly dependent on the particular copolymer. Indeed, a major factor in establishing the timescale of each run is the ultimate coverage, and this is seen to increase with increasing copolymer hydrophobicity. Further, the impact of bulk solution concentration on the ultimate coverage is greatest for the most hydrophilic copolymers, which may indicate a slightly weaker free energy of adsorption for these compounds. The most hydrophobic copolymers show coverages practically independent of bulk solution concentration indicating a strong driving force for adsorption. Acid-etched silica is, however, hydrophilic. While, silica adsorbs PEG via h-bonding, there is no substantial driving force for the adsorption of the PDMS backbone. Confinement within an adsorbed layer may, however, reduce any costs associated with hydrophobic aggregation, so that the hydrophobic portions of the chain tend to aggregate.

3.3. The adsorbing species

Analyses of the adsorption rates, which show protracted linearity on silica (typical of diffusion-limited adsorption behavior) in Fig. 2, via a transport-limited model allows identification of the adsorbing species (micelles, single chains, etc.) and a self consistency check of whether adsorption is indeed transport-limited. Fig. 3 summarizes the (initial) slopes for the all the runs and showcases their proportionality to the bulk solution concentration. This proportionality is linear in the dilute limit. A 1/3-power law dependence on wall shear rate, γ, is shown in part C. For transport-limited kinetics in slit-shear cells such as ours, the Leveque solution [48] to the convection diffusion equation relates the adsorption rate, $d\Gamma/dt$ to the bulk solution concentration, C; the wall shear rate, γ; and the diffusion coefficient, D, of the adsorbing species. (If multiple adsorbing species are present, the adsorption rate of each is described by this form.)

$$\frac{d\Gamma}{dt} = \frac{1}{\Gamma(4/3)9^{1/3}}\left(\frac{\gamma}{DL}\right)^{1/3} DC. \tag{1}$$

In Eq. (1), L is the distance from the entrance of the flow cell to the point of observation. Here and only here $\Gamma(4/3)$ in the denominator of the right-hand side is the gamma function evaluated at

an argument of 4/3. Equation (1) holds as long as the surface has sufficient capacity to accommodate incoming species, maintaining a linear pseudo-steady-state concentration gradient near the surface. This condition breaks down if the surface capacity is small such that the time to reach the pseudo-steady-state condition is longer than that to saturation the surface [49]. Applying the quantitative criterion of Lok et al. [49], we find the Leveque solution to hold exactly for concentrations below 100 or 200 ppm, depending on the which of the 4 copolymers we consider. In fact, we find, in some instances, the linearity in concentration to be sustained at higher concentrations, allowing us to proceed with the analysis with confidence.

From Eq. (1), in the dilute limit, we find the diffusion coefficients of the adsorbing species, in Fig. 4, and from the Stokes–Einstein relationship, the hydrodynamic radius of the adsorbing species, in Fig. 5. Of interest, in none of these cases are single chains or classical micelles dominant in the adsorption. Rather, the large aggregates, seen with static light scattering, are found here to dominate the development of the adsorbed layers. (Fig. 5 includes a schematic of what these aggregates might look like.) Indeed, the near-perfect agreement between the R_h values from adsorption/diffusion and $\langle S^2 \rangle_z^{1/2}$ from static light scattering is remarkable. This confirms transport-limited behavior for the periods in which the adsorption runs themselves were linear. (Without knowing the structure of the aggregates exactly, the quantitative relationship between R_g and R_h is difficult to anticipate, and is complicated by polydispersity. None the less, the fact that the values are, in all cases similar, suggests that the solution-phase structure is key to the interfacial build-up.) Also of note, the curvature in Fig. 3 for the rate dependence on the bulk concentration is qualitatively consistent with diffusion-limited adsorption, but without establishment of the pseudo-steady-state condition. That is, for times

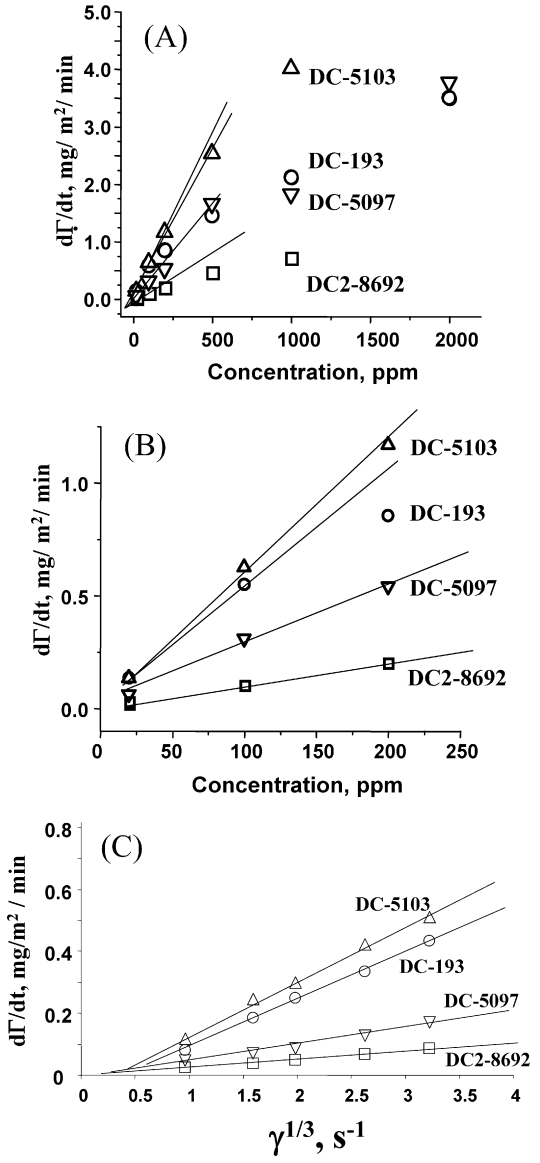

Fig. 3. (A) Initial adsorption kinetics for copolymers on silica. (B) In the dilute limit. (C) Wall shear rate dependence for 20 ppm solutions.

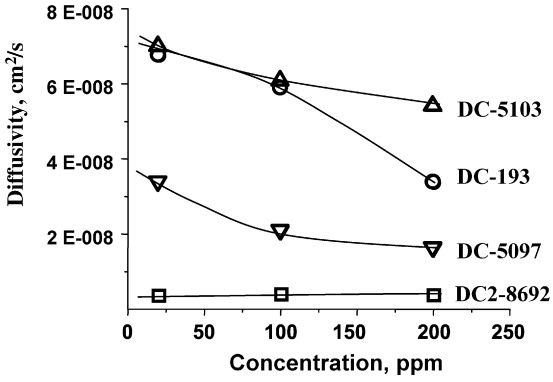

Fig. 4. Apparent diffusion coefficient of the adsorbing species, from Eq. (1) and the initial adsorption slopes.

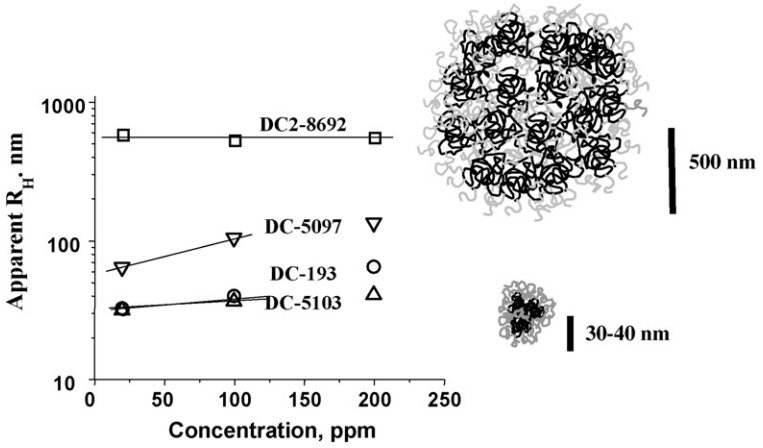

Fig. 5. Hydrodynamic radii of the adsorbing species, from data in Fig. 4 and Stokes–Einstein.

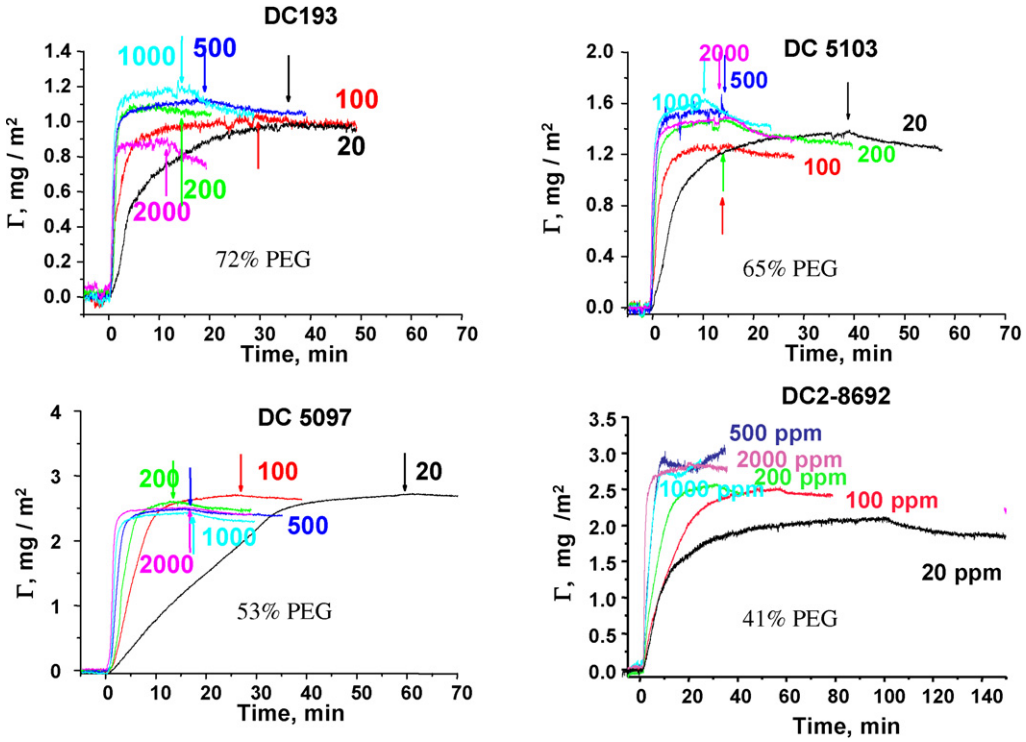

Fig. 6. Raw adsorption traces on C16 surface. A few data sets were eliminated for black and white viewing (DC-193 200 ppm; DC-5103 200 ppm; DC2-8692 500 ppm).

shorter than needed to establish the pseudo-steady-state concentration gradient that gives the adsorption kinetics described by Eq. (1), the adsorption kinetics are curved upwards. If the surface starts to saturate before pseudo-steady-state occurs, the kinetic plot then turns over and becomes concave down, approaching the saturation level without ever exhibiting the pronounced linearity seen at lower concentrations.

3.4. Kinetics and structure: C16 versus silica substrates

Fig. 6, which presents adsorption traces for the 4 copolymers on C16 surfaces, is qualitatively similar to Fig. 2 for adsorption on silica, with similar ultimate adsorbed amounts and layer resistance to rinsing. Indeed, the *initial* adsorption kinetics on C16 are identical to those on silica, such that Figs. 4 and 5 describe the adsorbing species on C16 as well. A quick look at Fig. 6 does not suggest surface-dependent differences in the layer structure; however, a closer examination reveals otherwise. Most notably, on C16, all the shoulders are rounded rather than sharp, as had been the case on silica. Especially for the DC-193 and DC-5103, the approach to surface saturation on C16 is protracted.

Fig. 7 compares the adsorption kinetics from 20 and 100 ppm solutions of DC-193 on silica and C16 surfaces. (The same effects are seen at higher concentrations, but more difficult to distinguish as pseudo-steady-state conditions begin to fail.) The same initial slopes on the two surfaces indicate transport-limited adsorption of the same 30 nm aggregates on bare silica and bare C16. On the C16 surface, however, the first 0.45–0.5 mg/m^2 of adsorbed copolymer hinders subsequent adsorption, while on silica, adsorption of the aggregates continues at the same rate until saturation. The particular value of 0.5 mg/m^2 on the C16 surface, where adsorption deviates from the transport limit, is independent of the bulk solution concentration, suggesting that the shoulder is a result of surface crowding. Indeed, this particular level of coverage is consistent with a mushroom-type interfacial structure, where non-adsorbed PEG tails adopt random coil conformations and are not dramatically stretched normal to the surface.

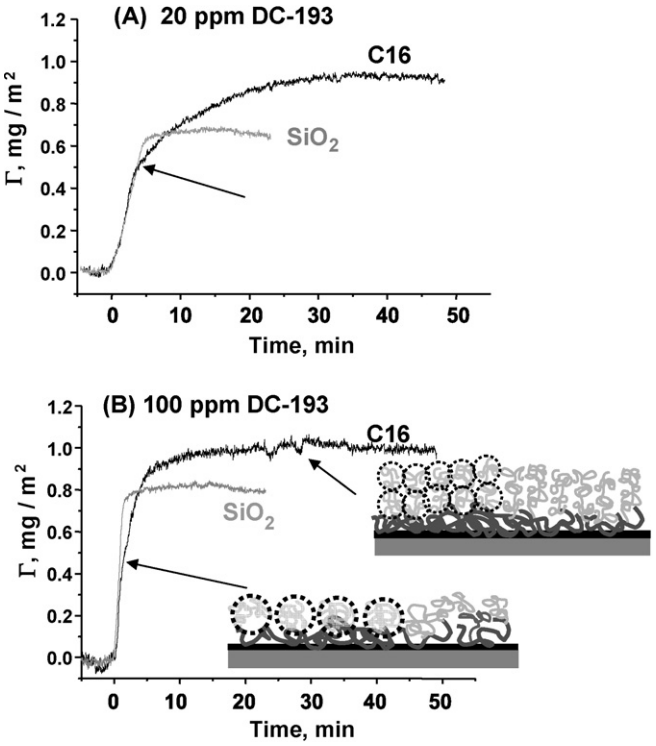

Fig. 7. Comparing adsorption kinetics of DC-193 on silica and C16 surfaces in the dilute limit. The 100 pm plot shows likely interfacial mushroom/brush structures on C16, which would occur for both bulk solution concentrations.

To see this further, we consider that the PDMS backbone will be preferred, over the PEG side chains, on the C16 surface. In the absence of substantial surface crowding, the solubilized PEG chains will adopt random coil conformations that define the fullness of the surface, per the definition of mushroom regime [50]. If, based on the amount of PEG in each DC-193 chain, we crudely estimate

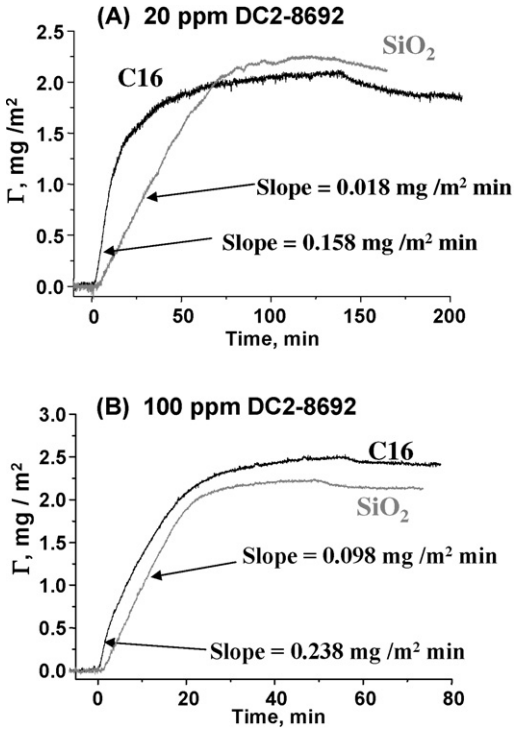

Fig. 8. Dilute regime adsorption behavior of DC2-8692 on both substrates, providing evidence for the adsorption of a small amount of a small species, only the hydrophobic surface.

a random coil footprint for each chain, we obtain $R_g = 0.84$ nm (from the size of an EO unit, 0.29 nm. (The radius of gyration for a PEG macromolecule was estimated from $R_g = a(N/6)^{1/2}$, where $a = 0.29$ nm and was calculated from the known end–end distance of 5.44 nm for PEG having $M_w = 5000$ [51].) If we then saturate the surface with spheres of this size, we get a coverage near 0.6 mg/m^2, consistent with our shoulder values of 0.5 mg/m^2. The interpretation is, then, that even though aggregates of DC-193 adsorb, they quickly relax on the C16 surface to present their PEG side-arms to the solution. Once the surface is shielded by a layer of PEG coils, additional adsorption requires penetration of this osmotic pressure barrier. This additional slower adsorption, however, produces a brushy surface. Indeed, the self-retarding nature of brush adsorption kinetics [21] is one of the reasons why the formation of robust brushes is difficult [52].

It is worth noting by contrast that the DC-193 adsorbing on silica, which exhibits linear kinetics (corresponding to the adsorption of 30 nm aggregates) until saturation, is unlikely to form a brush. On silica, the adsorption kinetics lack the self-retarding signature of brush formation. Of course, on silica, one does not expect the siloxane portions of the copolymer to contact the surface, as needed for a brush. For this reason, and because of the tendency of this polymer to aggregate in the first place, we interpret DC-193 adsorption to be accumulation of 30 nm aggregates, with the aggregated structure likely to persist in some form.

DC2-8692 presents a surprise in Fig. 8, which compares its adsorption from dilute solution on C16 and silica surfaces at 20 and 100 ppm. While the adsorption traces on silica display the usual linear transport-limited character, the early stage kinetics on the C16 surface are faster. This is unexpected because one thinks of the transport-limited rate (as reported on silica) as being the fastest possible. Indeed, the analysis of the DC2-8692 adsorption on silica in was convincing, because it identified the dominant adsorbing species to be the same nearly 500 nm aggregate seen in solution via light scattering. Adherence to the 1/3-power scaling law for shear rate (in Fig. 3C) was further evidence for transport-limited adsorption.

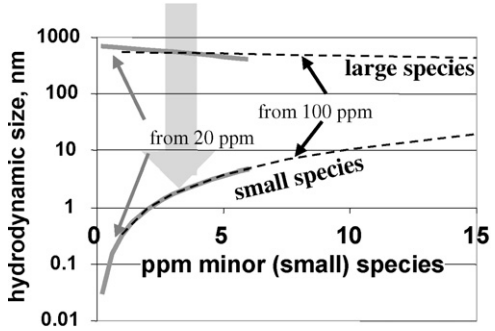

Fig. 9. Sizes of large and small adsorbing species in DC2-8692, as calculated from a mass balance and the slopes of DC2-8692 on C16 and silica surfaces at 20 and 100 ppm runs.

A quantitative analysis reveals, however, transport limited kinetics on both surfaces, if multiple species are allowed. Our simplified analysis describes the DC2-8692 solution as a bimodal mixture, containing large (approximately 500 nm) aggregates as the major species, and a smaller species, present at lower concentrations and difficult to detect by light scattering. Apparently, only the large 500-nm aggregates adsorb on silica. Both species, however adsorb onto the C16 surface initially, with the small species dominating the kinetics because it is faster, even though it is the minor component. At longer times on the C16 surface, the smaller species cannot access the surface well and only the large species continues to adsorb. Indeed, at 100 ppm, the late stage kinetics on the C16 exhibit the same slope as was seen during the entire adsorption process on silica, indicating that here, the large species dominate.

The nature and amount of the small species in DC2-8692 was probed by repeated applications of Eq. (1) to 20 and 100 ppm data sets, on silica and on C16. For instance, one might guess that the 100 ppm solution is made up of 5% by weight (5 ppm) of the small species. Then, using the observed initial adsorption rates on the C16 and silica surfaces, and by allowing the initial adsorption (fast) rate on the C16 surface to be the sum of the rates for the large and small species, (while the adsorption rate on the silica surface to be only the large species), one arrives at a small species size of 3.7 nm, and a large species size of 518 nm. The dashed lines in Fig. 9 show how the sizes of the adsorbing species depend on the possible content of the small species. A similar analysis was done for the 20 ppm solution, using the observed adsorption rates on the two surfaces. Key in this analysis is the observation that the fast initial kinetic regime on the C16 surface contributes to a progressively smaller fraction of the surface coverage as the bulk solution concentration increases. This suggests that with increases in bulk solution concentration, the small species is an increasingly less significant fraction of the bulk solution, much like the impact of single molecules in a micelle-forming system. We therefore approximated the concentration of the small species to be constant, but its concentration fraction to decrease as the solution concentration was increased from 20 and 100 ppm. With this constraint, Fig. 9 superposes the solutions to Eq. (1) on the same plot (the gray lines). The sets of gray and dashed lines are similar but one can identify where the two cross, for the small and large species, conforming to the constraint that the minor species is present at the same concentrations in the two solutions. The solution (essentially 4 transport equations and 4 unknowns) is shown by the wide vertical arrow, whose width indicates reasonable error in the calculation. The finding is that only about 3 ppm of the minor species exist, and it is only about 2 nm in size. Inclusion of the minor species also only affects the size of the major species slightly, so

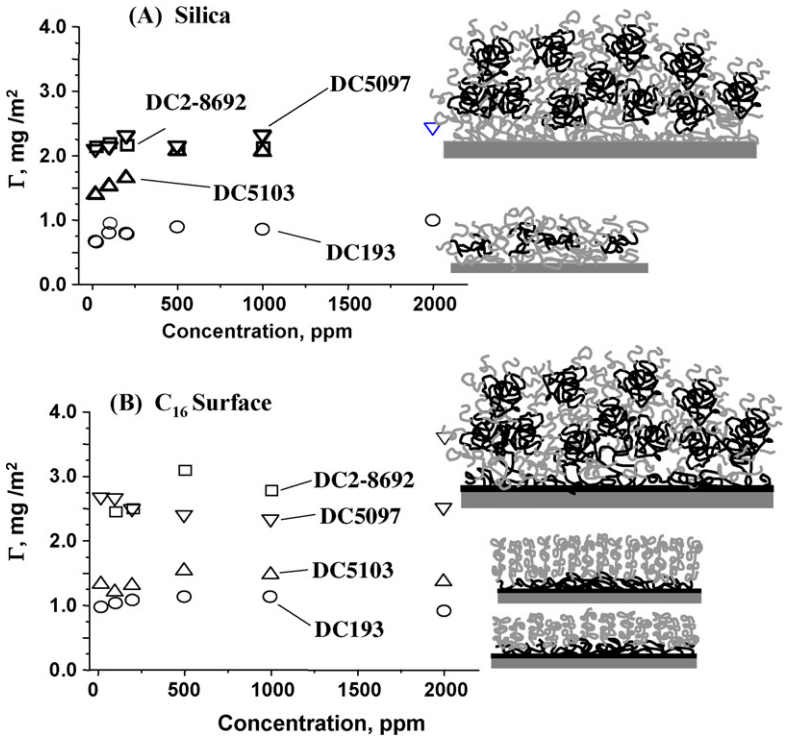

Fig. 10. Coverages and likely layer structures on (a) silica (b) C16.

that the values reported in Figs. 4 and 5 are essentially still correct for the large species of DC2-8692.

Fig. 9 is intended only to provide a ballpark estimate of the concentrations and roles of the different species in DC2-8692 on the C16 surface. Its take-home point is that the amount of the small species is very small, and yet it has a huge impact on adsorption from the most dilute solutions. From the surface tension data in Fig. 1, one might expect all the surfactant formulations to contain a minor amount of a similarly small species; however, Fig. 9 argues against this. In none of the other 3 formulations did we observe fast (for small species) dilute-solution-limited kinetics. This means that any small species in DC-193, DC-5103, or DC-5097 that adsorbs in the dilute limit does so in the same proportions on the hydrophilic and hydrophobic surfaces. Further any minor species must continue to adsorb in the same proportion initially and up to saturation. With these constraints, the adsorption of a minor species will reduce the average apparent sizes of the adsorbing species in Figs. 4 and 5. Indeed Fig. 9 argues that even a small amount of such a small species would have a huge effect on the apparent size of the adsorbing aggregate. The agreement between Fig. 5 and Table 2 therefore suggests that any adsorbing small species in any of the solution is present to no more than a parts per million.

3.5. Layer coverage and structure

Fig. 10 shows modest influence of substrate hydrophobicity on the ultimate copolymer adsorption. Coverages are slightly greater on the C16 surface. Coverage levels alone provide minimal insight into the adsorbed layer structure; however, when combined with the adsorption kinetics above, we can say more about the probable layer structure.

On silica in Fig. 10A, the flatness of the pseudo-isotherms is consistent with the high affinity binding and resistance of the copolymer layers to buffer washes. Since we find only reversible adsorption of low molecular weight PEG on silica, the hydrophobic PDMS backbones must be responsible for the strong binding and the relatively high coverages of the copolymers on silica relative to pure PEG. We do not expect attractions between the silica and the siloxane backbone, and therefore conclude that the elevated coverages with the 4 copolymers are due to hydrophobic associations within the adsorbed layers, with the PEG being the entity that binds to the silica surface. That is, the effect of the hydrophobic associations is to increase the effective PEG molecular weight. Indeed, high molecular weight PEO adsorbs to silica through hydrogen bonding and can be extremely difficult to rinse away or displace through the exchange of like polymer [53,54]. Also, associative polymers with modest molecular weight PEO and smaller hydrophobes show elevated coverages on silica compared with that of pure PEO [55]. Such interfacial associations and micelles have been seen for other PEG–siloxane surfactants on hydrophilic mica [31]. Fig. 10A therefore includes a schematic of the potential layer structure on silica.

On C16. The slightly elevated coverages on the C16 surfaces (relative to silica) and the detailed kinetic traces suggest a variety of structures on the C16 surfaces. Indeed the DC-193 and DC-5103, with their protracted approach to saturation likely approach polymer brush structure. Above, we calculated that the surface coverage toward the end of the mushroom regime for DC-193 should be 0.5–0.6 mg/m^2. In Fig. 10B, the plateau coverages of twice this value suggest a semi-brush with 2 or so "blobs," indicating slight stretching of the PEG into solution, with an energy of 2 kT. A brush structure for the DC-5103, with its higher coverage (relative to the DC-193), implies a more extended PEG chain conformation of 3–4 blobs and about 3–4 kT of stretching energy (1 kT/"blob"). Hence the DC-193 is likely to form a fledgling brush while the DC-5103, with its slightly greater hydrophobic content and stronger binding energy, more closely approaches a true brush.

DC-5097 and DC2-8692, with their greater relative hydrophobicity and stronger potential binding to the C16 surface would seem to be able to form more extended brushes (though at some point the size of the hydrophobic PDMS footprint on the surface will limit the crowding of PEG chains in the fluid adjacent to the surface). The adsorption kinetics, however, indicate non-brush

structure, as the adsorption timescales on the C16 surface are more nearly similar to those on silica than was the case for DC-193 or DC-5103. Self retarding kinetics are prerequisite to brush formation [21]. Even the DC2-8692, which exhibits bimodal kinetics on C16, shows a linear approach to surface saturation. This indicates that for the DC-5097 and DC2-8692, adsorption of large aggregates proceeds at the transport limited rate until the surface is saturated. There is no evidence that a growing brush hinders surface saturation. However, it is possible that beneath the adherent on the C16 surface there lies a mushroom-regime layer, which contains hydrophobic imperfections. By the latter we mean that either (1) the hydrophobic trains which adsorb to the C16 are insufficiently shielded by the small PEG chains, providing a driving force for aggregate adsorption, or (2), portions of the hydrophobic backbone loop from the surface to associate with hydrophobic regions on adsorbing aggregates. In summary, we believe that the DC-193 and DC-5103 adsorb to form semi-brushes, while the more hydrophobic copolymers form layers of aggregates beneath which, on the C16 surface, may exist an imperfect brush.

4. Discussion and summary

On both silica and C16 surfaces, the adsorption of all 4 copolymers was sufficiently strong to resist rinsing in pH 7 buffer, and the coverages were higher than one would expect for simple adsorbed layers of low molecular weight (homopolymer-type structures of tails, loops, and trains, order 0.5 mg/m^2 or less.) This, combined with the observation of increasing coverage with copolymer hydrophobicity on both surfaces, argues for interfacially associated structures on the hydrophilic surfaces (where the PEG is favored to interact more directly with the silica than would the PDMS) and associations or brushes on the C16 surfaces, where the PDMS should dominate the train layer. Arguments for these layer types are further strengthened by the kinetic data. First, the transport-limited initial slopes for all the systems are in agreement with light scattering for the aggregates sizes, identifying aggregates as the dominant adsorbing species even in very dilute solutions. The question, then, is the extent to which these aggregates remain, after arrival to the interface.

On the silica, with its established affinity for PEO/PEG adsorption, the exterior of the aggregates will adhere, and indeed, Fig. 2 indicates for all 4 copolymers that aggregate capture by silica proceeds linearly at the transport-limited rate over the full course of adsorption. This linearity-to-saturation is at odds with the development of a brush (as interfacial mass accrues) because the developing brush provides an osmotic barrier to further adsorption. This is the case for penetration of single chains into a growing brush, and it will also be the case for colloidal scale aggregates whose surfaces are sterically-stabilized by PEG chains. Thus, the process of adsorption on silica is, for all four copolymers, one of continued aggregate accumulation on the surface, with no evidence for other interfacial restructuring. If such relaxations do occur, they would appear to be independent of the accrual of interfacial mass; however, there is a precident for PEG–siloxane aggregates and micelles on hydrophilic surfaces [31–33]. Therefore, the simplest picture of the adsorbed layers on silica is one involving persistent aggregates.

On the C16 surface, the PDMS is expected to dominate the copolymer-substrate contact, providing potential for brush formation. We have confirmed, independently, that PEG/PEO will also adsorb substantially on C16 surfaces (even with molecular weights as low as 4500), and are therefore comfortable with the initial transport-limited capture of aggregates by their outer coronas, when the C16 surfaces are nearly bare. Following the initial transport-limited kinetics of the DC-193 and DC-5103, the slower subsequent adsorption, and the slightly higher coverages compared with the same copolymers on silica are consistent with modest brush formation on C16 surfaces.

Finally, the copolymers with greater hydrophobicity, DC-5097 and DC2-8692, show adsorption kinetics similar to those on silica, with transport-limited behaviors, though the DC2-8692 is complicated by bimodal kinetics. The lack of a substantial slowdown much before saturation suggests rapid acceptance of entire aggregates into the adsorbed layer and the potential retention of these structures. The slightly higher coverages of these copolymers on C16 surface compared with silica suggests, however that beneath several mg/m^2 of aggregated structure lies approximately 0.5 mg/m^2 of mushroom-structured layer, or a layer in which both PEG and PDMS contact the surface. The copolymer molecules nearest the surface must be sufficiently accessible to aggregates from solution to promote further aggregate adhesion and retention of such structures.

In summary, all 4 copolymers produce aggregated structures on silica, with surface coverages increasing with copolymer hydrophobic content. On the C16 surface, the more hydrophilic copolymers with 72 and 65% PEG form brushes (albeit rather short), and the more hydrophobic copolymers form aggregated layers, likely on top of a mushroom-like or mixed adsorbed layer. It turns out, as we report separately in detail, that all the copolymer layers retard protein adsorption at short times (order hours), but only those possessing brush structure, truly reduce protein adsorption to zero (order 0.01 mg/m^2) on these timescales.

Acknowledgments

This work was supported by a Grant from Becton-Dickinson Corporation. W. Reed and A. Alb gratefully acknowledge support and donations and loans of instruments from Shimadzu, Arkema, Inc., Total S.A., Polymer Laboratories Ltd., Brookhaven Instruments Corporation, Tulane University, and UMass MRSEC (DMR-0213695) during their stay at UMass in the wake of Hurricane Katrina in August 2005, which closed Tulane University for several months.

References

[1] K. Matyjaszewski, J.H. Xia, Chem. Rev. 101 (2001) 2921–2990.
[2] W.J. Brittain, S. Minko, J. Polym. Sci. Part A Polym. Chem. 45 (2007) 3505–3512.
[3] G.L. Kenausis, J. Voros, D.L. Elbert, N.P. Huang, R. Hofer, L. Ruiz-Taylor, M. Textor, J.A. Hubbell, N.D. Spencer, J. Phys. Chem. B 104 (2000) 3298–3309.
[4] J.M. Brockman, A.G. Frutos, R.M. Corn, J. Am. Chem. Soc. 121 (1999) 8044–8051.
[5] S.J. Sofia, V. Premnath, E.W. Merrill, Macromolecules 31 (1998) 5059–5070.
[6] M. Malmsten, K. Emoto, J.M. Van Alstine, J. Colloid Interface Sci. 202 (1998) 507–517.
[7] T. McPherson, A. Kidane, I. Szleifer, K. Park, Langmuir 14 (1998) 176–186.
[8] J.H. Lee, B.J. Jeong, H.B. Lee, J. Biomed. Mater. Res. 34 (1997) 105–114.
[9] M. Ulbricht, H. Matuschewski, A. Oechel, H.G. Hicke, J. Membr. Sci. 115 (1996) 31–47.
[10] K. Bergstrom, K. Holmberg, A. Safranj, A.S. Hoffman, M.J. Edgell, A. Kozlowski, B.A. Hovanes, J.M. Harris, J. Biomed. Mater. Res. 26 (1992) 779–790.
[11] J.L. Dalsin, L.J. Lin, S. Tosatti, J. Voros, M. Textor, P.B. Messersmith, Langmuir 21 (2005) 640–646.
[12] R. Fukai, P.H.R. Dakwa, W. Chen, J. Polym. Sci. Part A Polym. Chem. 42 (2004) 5389–5400.
[13] X. Gong, L. Dai, H.J. Griesser, A.W.H. Mau, J. Polym. Sci. Part B Polym. Phys. 38 (2000) 2323–2332.
[14] S.J. Sofia, E.W. Merrill, J. Biomed. Mater. Res. 40 (1998) 153–163.
[15] S. Herrwerth, W. Eck, S. Reinhardt, M. Grunze, J. Am. Chem. Soc. 125 (2003) 9359–9366.
[16] A.J. Pertsin, M. Grunze, I.A. Garbuzova, J. Phys. Chem. B 102 (1998) 4918–4926.
[17] P. Harder, M. Grunze, R. Dahint, G.M. Whitesides, P.E. Laibinis, J. Phys. Chem. B 102 (1998) 426–436.
[18] E. Mubarekyan, M.M. Santore, Macromolecules 34 (2001) 7504–7513.
[19] K. Schillen, P.M. Claesson, M. Malmsten, P. Linse, C. Booth, J. Phys. Chem. B 101 (1997) 4238–4252.
[20] C. Amiel, M. Sikka, J.W. Schneider, Y.H. Tsao, M. Tirrell, J.W. Mays, Macromolecules 28 (1995) 3125–3134.
[21] S.T. Milner, Macromolecules 25 (1992) 5487–5494.
[22] A. Johner, J.F. Joanny, Macromolecules 23 (1990) 5299–5311.

[23] D. Perahia, D.G. Wiesler, S.K. Satija, L.J. Fetters, S.K. Sinha, G.S. Grest, Physica B 221 (1996) 337–341.
[24] S.T. Milner, Science 251 (1991) 905–914.
[25] M.S. Kent, L.T. Lee, B.J. Factor, F. Rondelez, G.S. Smith, J. Chem. Phys. 103 (1995) 2320–2342.
[26] E.S. Pagac, D.C. Prieve, Y. Solomentsev, R.D. Tilton, Langmuir 13 (1997) 2993–3001.
[27] T. Svitova, H. Hoffmann, R.M. Hill, Langmuir 12 (1996) 1712–1721.
[28] A.D. Nikolov, D.T. Wasan, A. Chengara, K. Koczo, G.A. Policello, I. Kolossvary, Adv. Colloid Interface Sci. 96 (2002) 325–338.
[29] S. Zhu, W.G. Miller, L.E. Scriven, H.T. Davis, Colloids Surf. A Physicochem. Eng. Aspects 90 (1994) 63–78.
[30] K.P. Ananthapadmanabhan, E.D. Goddard, P. Chandar, Colloids Surf. 44 (1990) 281–297.
[31] J.P. Dong, G.Z. Mao, R.M. Hill, Langmuir 20 (2004) 2695–2700.
[32] T. Svitova, R.M. Hill, C.J. Radke, Colloids Surf. A Physicochem. Eng. Aspects 183 (2001) 607–620.
[33] Y.N. Lin, T.W. Smith, P. Alexandridis, Langmuir 18 (2002) 6147–6158.
[34] Y.N. Lin, T.W. Smith, P. Alexandridis, J. Colloid Interface Sci. 255 (2002) 1–9.
[35] R. Toomey, J. Mays, M. Tirrell, Macromolecules 39 (2006) 697–702.
[36] I. Szleifer, M.A. Carignano, Macromol. Rapid Commun. 21 (2000) 423–448.
[37] K. Eskilsson, F. Tiberg, Macromolecules 30 (1997) 6323–6332.
[38] F.A.M. Leermakers, A.P. Gast, Macromolecules 24 (1991) 718–730.
[39] M.R. Munch, A.P. Gast, J. Chem. Soc. Faraday Trans. 86 (1990) 1341–1348.
[40] M.R. Munch, A.P. Gast, Macromolecules 23 (1990) 2313–2320.
[41] A.P. Gast, M.R. Munch, Colloids Surf. 31 (1988) 47–50.
[42] P. Brandani, P. Stroeve, Macromolecules 36 (2003) 9492–9501.
[43] B. Zdyrko, P. Ofir, M.M. Santore, Biomacromolecules, in preparation.
[44] Z.G. Fu, M.M. Santore, Colloids Surf. A Physicochem. Eng. Aspects 135 (1998) 63–75.
[45] G.A. Sorci, W.F. Reed, Langmuir 18 (2002) 353–364.
[46] R. Strelitzki, W.F. Reed, J. Appl. Polym. Sci. 73 (1999) 2359–2367.
[47] M. Kerker, The Scattering of Light and Other Electromagnetic Radiation, Academic Press, New York, 1963.
[48] M.A. Leveque, Ann. Mines 13 (1928) 284.
[49] B.K. Lok, Y.L. Cheng, C.R. Robertson, J. Colloid Interface Sci. 91 (1983) 104–116.
[50] S. Alexander, J. De Phys. 38 (1977) 983–987.
[51] J. Brandrup, E.H. Immergut, E.A. Grulke, Polymer Handbook, fourth ed., Wiley, New York, 1999.
[52] M.S. Kent, L.T. Lee, B. Farnoux, F. Rondelez, Macromolecules 25 (1992) 6240–6247.
[53] E. Mubarekyan, M.M. Santore, Macromolecules 34 (2001) 4978–4986.
[54] Z.L. Fu, M. Santore, Macromolecules 32 (1999) 1939–1948.
[55] Y.D. Huang, M.M. Santore, Langmuir 18 (2002) 2158–2165.